JMSR 1(3) (2025)

Journal of Material Science and Radiation

https://journals.balaipublikasi.id/jmsr

Influence of Sintering Temperatures on $Pr_{0.7}Ba_{0.3}MnO_3$ Prepared Using Thermal Treatment Method

Xiao Tong Hon[1], Kean Pah Lim[1*], Lik Nguong Lau[1,2], Mohd Mustafa Awang Kechik[1], Soo Kien Chen[1], Muhammad Kashfi Shabdin[1], Nurhidayah Mohd Hapipi[1], Najihah Rohiat[1], Abdul Halim Shaari[1]

[1] Superconductor and Thin Film Laboratory, Department of Physics, Faculty of Science, Universiti Putra Malaysia, 43400 UPM Serdang, Selangor Darul Ehsan, Malaysia.
[2] International College of Semiconductor Technology, National Yang Ming Chiao Tung University, Hsinchu, 30010, Taiwan

Received: October 17, 2025
Revised: November 29, 2025
Accepted: December 25, 2025
Published: December 31, 2025

Corresponding Author:
Kean Pah Lim
limkp@upm.edu.my

DOI: 10.56566/jmsr.v1i3.478

Abstract: In this work, $Pr_{0.7}Ba_{0.3}MnO_3$ (PBMO) was synthesised using a thermal treatment method with sintering temperature ranging from 800 °C to 1100 °C. X-ray diffraction (XRD) confirmed the formation of pure PBMO phase at 1100 °C, while lower sintering temperatures led to the presence of secondary phase, particularly $Pr(Mn_2O_5)$. Microstructural analysis revealed significant grain growth with rising sintering temperatures, accompanied by enhanced crystallinity and reduced secondary phases. Magnetic measurements indicated ferromagnetic behaviour at room temperature for all samples. However, the electrical resistivity demonstrates an unexpected increase with sintering temperature, attributed to the influence of secondary phase at lower sintering temperatures and grain growth in the pure PBMO phase at higher sintering temperatures. Additionally, microstructural defects such as oxygen non-stoichiometry or porosity might further contribute to the suppression of the metal-insulator transition temperature. Overall, this study highlights the significant role of sintering temperatures in controlling the phase purity, microstructure and physical behaviour of PBMO samples, offering valuable insights for their potential applications in spintronics or magnetic sensing devices.

Keywords: Grain boundaries; Grain growth; Microstructural defects; Oxygen stoichiometry; Pr-based manganites.

Introduction

Manganite materials have garnered significant attention in material science owing to their unique interplay of charge, spin, orbital and lattice degrees of freedom, which give rise to intriguing phenomena such as colossal magnetoresistance and significant magnetocaloric effect (Mohamed et al., 2020; Xia et al., 2020). Additionally, their ability to fine-tune the Curie temperature (T_C) close to room temperature through substitutions further enhances their potential for applications in magnetic refrigeration, spintronics and magnetic sensors (M'nassri et al., 2017; Telegin & Sukhorukov, 2022).

Among the various rare-earth elements, Pr-based manganites have emerged as as prominent subjects of study due to their interesting magnetic behaviour. These materials behave like antiferromagnetic insulators near the Neel temperature and displays anisotropic characteristics below this temperature (Hanen et al., 2020). Moreover, substituting praseodymium for lanthanum at the rare-earth site in the perovskite structure significantly improves the electrical conductivity (Matheswaran et al., 2017). In particular, this replacement of the non-magnetic La^{3+} ions with isovalent Pr^{3+} reduces Mn-O-Mn bond angles, resulting in more carrier localisation (Christopher et al., 2018).

In this study, the incorporation of barium (Ba^{2+}) into Pr-based manganite is expected to introduce additional complexities into the system. Barium ions, with their larger ionic size compared to praseodymium ions, create a high mismatch between the lanthanide and barium ionic radii (Ur Rehman et al., 2015). This mismatch induces lattice distortion and strain effects, which can

How to Cite:
Hon, X. T., Lim, K. P., Lau, L. N., Kechik, M. M. A., Chen, S. K., Shabdin, M. K., … Shaari, A. H. Influence of Sintering Temperatures on Pr0.7Ba0.3MnO3 Prepared Using Thermal Treatment Method. *Journal of Material Science and Radiation*, *1*(3), 98–103. https://doi.org/10.56566/jmsr.v1i3.478

strongly alter the magnetic and electrical behaviour of the materials (Khelifi et al., 2017).

Preparation methods and sintering temperatures are critical factors influencing the microstructural modifications and, consequently, the physical properties of manganites (Ayadi et al., 2018; Shlapa et al., 2018). This work is particularly novel as it reports the first successful synthesis of Pr-based manganites using a new developed thermal treatment method, previously applied by our research group only to Nd-based manganites (Hon et al., 2023). Additionally, the effects of sintering temperatures, ranging from 800 °C to 1100 °C were systematically studied to understand their impact on crystallinity, microstructural evolution, and overall physical behaviour of the manganite materials.

Method

In this study, $Pr_{0.7}Ba_{0.3}MnO_3$ (PBMO) was synthesised using thermal treatment method, as previously reported by our group (Hon et al., 2024; Hon et al., 2023). The starting powders included praseodymium (III) acetate hydrate (Alfa Aesar, 99.9 %), barium nitrate (Alfa Aesar, 99.95 %), and manganese (II) nitrate tetrahydrate (Sigma Aldrich, >97.0 %). These precursor powders were dissolved in distilled water according to their stoichiometric ratio, with 20 wt% of polyvinyl pyrrolidone (PVP) added to the solution and then stirred at 80 °C for 2 hours. The mixture was dried at 90 °C for 24 hours, followed by calcination at 500 °C for 5 hours. The calcined powder was ground using a pestle and mortar, before pressed into pellets using a hydraulic press. The pellets were subsequently sintered at temperatures ranging from 800 °C to 1100 °C.

The samples are referred to as PBMO 8, PBMO 9, PBMO 10, and PBMO 11, corresponding to their respective sintering temperatures. For sample characterisation, phase formation was identified using an X-ray diffractometer (XRD, X'Pert PRO PW 3040), and the microstructural behaviour was analysed using a scanning electron microscope (SEM, Phenom ProX G6). Additionally, the magnetic properties were measured using a vibrating sample magnetometer (VSM, Lakeshore 7407), while electrical analysis was conducted using a standard four-point probe method with a Cryostat Industries cryostat system in conjunction with a KEITHLEY current source and nanovoltmeter.

Result and Discussion

The X-ray diffraction (XRD) patterns of PBMO samples are shown in Figure 1, and the corresponding structural parameters obtained from Rietveld refinement are listed in Table 1.

Table 1. XRD data for PBMO samples sintered at different temperatures using thermal treatment method

Sample code	PBMO 8	PBMO 9	PBMO 10	PBMO 11
Phase	Praseodymium Barium Manganese Oxide, $Pr_{0.7}Sr_{0.3}MnO_3$			
Reference code	98-010-9966			
Structure type	Orthorhombic			
Space group	I m m a (74)			
a (Å)	5.514	5.517	5.524	5.524
b (Å)	7.751	7.761	7.772	7.775
c (Å)	5.492	5.494	5.499	5.502
V (Å)	234.715	235.242	236.066	236.312
Mn_1-O_1 (Å)	1.950	1.950	1.953	1.953
Mn_1-O_2 (Å)	1.970	1.973	1.975	1.976
Mn_1-O_1-Mn_1 (°)	172.705	172.699	172.698	172.697
Mn_1-O_2-Mn_1 (°)	159.125	159.145	159.153	159.150
R_{EXP} (%)	3.454	4.042	3.660	3.462
R_P (%)	5.445	4.667	4.051	3.580
R_{WP} (%)	8.068	6.220	5.426	4.875
χ^2	5.458	2.367	2.197	1.983
D (nm)	31.0	37.1	48.7	57.1
Phase	Praseodymium Mangano (III) Manganate (IV), Pr (Mn_2O_5)			
Reference code	98-007-6124			
Structure type	Orthorhombic			
Space group	P b a m (55)			
a (Å)	7.753	7.516	7.521	-
b (Å)	8.715	8.661	8.689	-
c (Å)	5.699	5.718	5.745	-
V (Å)	374.083	372.267	375.466	-

The quality of fit between the experimental data and the reference pattern is indicated by the goodness of fitting (χ^2). All samples exhibit the PBMO phase with an orthorhombic structure and Imma spare group as their main phase (ICSD code: 98-010-9966). In this study, a pure PBMO phase was achieved only at the sintering

temperature of 1100 °C, while samples sintered at lower temperatures exhibited secondary phases. As shown in Figure 1, the secondary phase, Pr (Mn_2O_5) was detected in PBMO 8, PBMO 9 and PBMO 10. This can be possibly caused by the insufficient thermal energy for complete phase formation (Fan et al., 2014). This observation is supported by the χ^2 values in Table 1, where the smallest χ^2 value for PBMO 11 implies better fitting due to the absence of secondary phases.

The lattice parameters also show noticeable changes in PBMO 8, PBMO 9 and PBMO 10, suggesting that the presence of secondary phases influences the crystal structure (Dippong et al., 2022). Thus, it can be deduced that crystallinity improves with increasing sintering temperature. The crystallite size, D was calculated using Scherrer's equation (Aguilar et al., 2020):

$$D = \frac{k\,\lambda}{\beta\,\sin\theta} \quad (1)$$

where k is the crystallite shape factor (0.9), λ represents the wavelength of X-ray (1.5406 Å), β stands for the full width at half maximum, and θ denotes the Bragg angle. As the sintering temperature increases, the crystallite size grew from 31.0 nm to 57.1 nm. This growth occurs because smaller crystals redeposit onto larger ones, and enhancing overall crystallite development (Bouzayen et al., 2023).

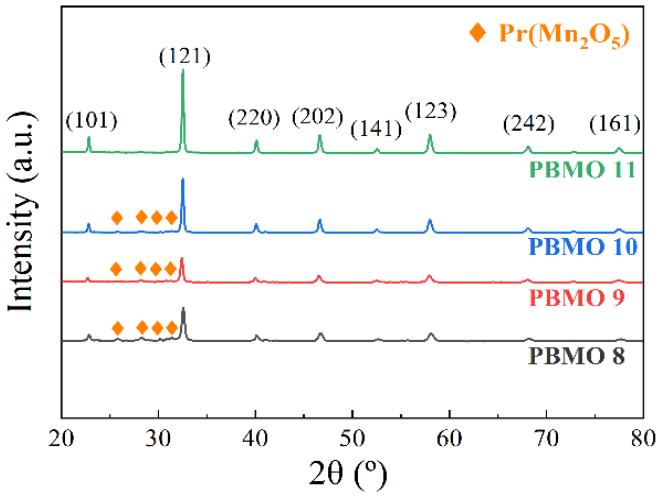

Figure 1. XRD patterns of PBMO samples with different sintering temperatures

Figure 2 illustrates the microstructural evolution of PBMO samples subjected to different sintering temperatures. In PBMO 8, the micrograph reveals agglomerated fine particles with unclear grain boundaries and non-uniform distribution, likely due to the presence of the secondary phase or incomplete compound formation at lower sintering temperature (Malti et al., 2021). In PBMO 9, the grains appear more homogeneous, and initial grain growth becomes noticablt. This observation aligns with the XRD analysis, where the peak intensity of the Pr (Mn_2O_5) diminishes with rising sintering temperature. As the sintering temperatures increase further, PBMO 10 exhibits significant grain enlargement and neck formation between adjacent grains. At the highest sintering temperature, PBMO 11 shows large, well-defined grains with clear grain boundaries, consistent with the XRD result indicating the formation of pure PBMO phase in the sample.

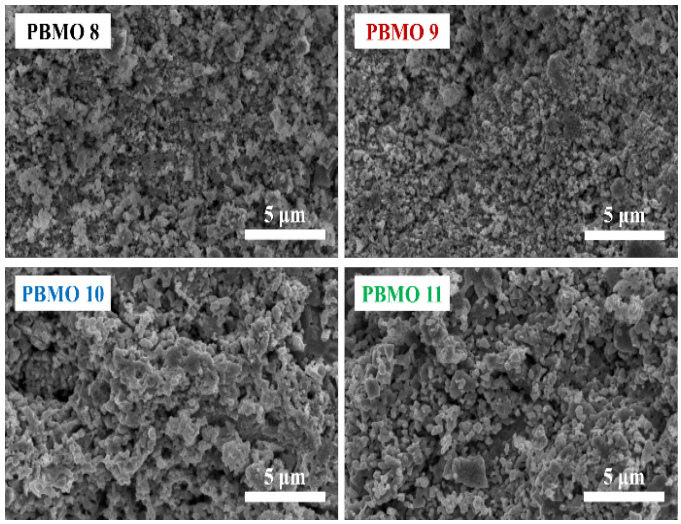

Figure 2. SEM micrographs of PBMO samples with different sintering temperatures

Field-dependent magnetisation (*M-H*) measurement of PBMO samples sintered at different temperatures were performed at 300 K, as depicted in Figure 3. All samples exhibit clear hysteresis loops, indicating ferromagnetic behaviour at room temperature (Taboada-Moreno et al., 2020). In other words, this suggests that the Curie temperature (T_C) of the PBMO samples prepared using this newly developed thermal treatment approach is above room temperature, in contrast to previous report of T_C around 184 K (Gamzatov et al., 2023). This discrepancy may arise from variations in synthesis conditions or microstructure features. Furthermore, the saturation magnetisation was found to increase with sintering temperatures, mainly because larger grains experience weaker surface effect due to a smaller surface-to-volume ratio (Lakouader et al., 2023). According to Shogh and Eshraghi (2019), only the core of the particles significantly contributes to magnetisation, as the overall magnetic behaviour of manganites is mainly governed by the ferromagnetic interactions within the particle cores. Therefore, as the sintering temperature increases and larger grains are formed, the contribution from the cores becomes more dominant, resulting in higher saturation magnetisation. In addition, the open hysteresis loop observed in the first quadrant of the *M-*

H curves for all samples may be related to the magnetic anisotropic effects (Zhang et al., 2018).

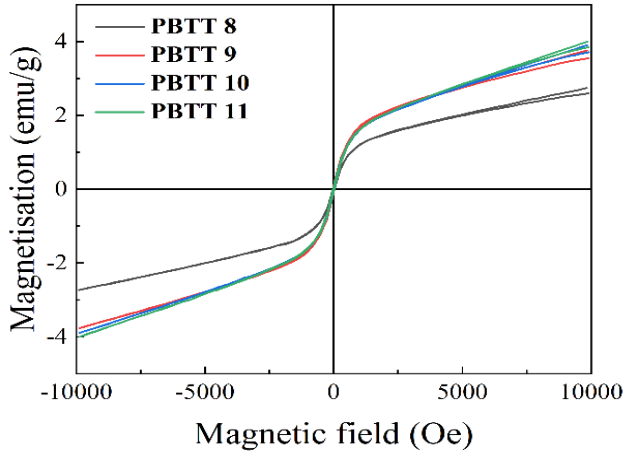

Figure 3. M-H curves at 300 K for PBMO samples with different sintering temperatures

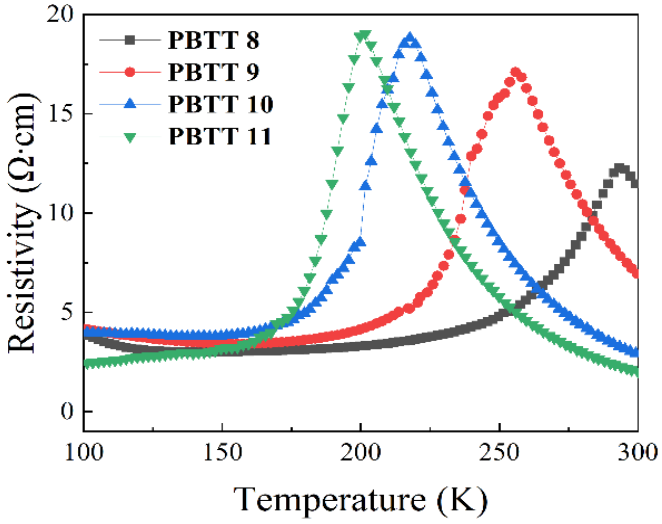

Figure 4. Resistivity as a function of temperature for PBMO samples with different sintering temperatures

Figure 4 displays the temperature-dependent resistivity (ρ-T) curves for PBMO samples sintered at various temperatures. As the sintering temperatures increased from 800 °C to 1100 °C, the peak resistivity gradually rose from 12.3 Ω.cm to 19.0 Ω.cm, while the metal-insulator transition temperature (T_{MI}) declined from 293 K to 202 K. Generally, higher sintering temperatures are expected to have lower resistivity due to grain size enlargement and the diminished impact of grain boundaries (Hizi et al., 2022; Ling et al., 2020; Wang et al., 2024). However, this study discovered an unusual increase in resistivity with rising sintering temperatures, which may be attributed to the presence of secondary phases. The Pr(Mn_2O_5) phase, in particular, might act as a barrier to charge carrier transport and disrupts the conduction paths (dos Santos-Gómez et al., 2024). Conversely, in PBMO 11, which contains only a single PBMO phase, the formation of larger grains at elevated sintering temperature boosts the driving force and grain boundary energy, leading to higher resistivity (Wu et al., 2021). Changes in T_{MI} could also be affected by microstructural defects or variations in oxygen stoichiometry (Kekade et al., 2019). In this thermal treatment method, higher sintering temperatures may cause oxygen loss or excess oxygen incorporation, resulting in increased scattering and higher resistivity (Qi et al., 2021). Furthermore, microstructural alterations such as phase composition or porosity might further contribute to the observed suppression of T_{MI}.(Ngida et al., 2019; Rosić et al., 2015).

Conclusion

In this work, $Pr_{0.7}Ba_{0.3}MnO_3$ (PBMO) was successfully synthesised using novel thermal treatment method with different sintering temperatures from 800 °C to 1100 °C. The results reveal that sintering temperature strongly influences the phase formation, microstructural evolution, magnetic properties and electrical behaviour of PBMO samples. XRD analysis confirmed that a pure PBMO phase was obtained only at the highest sintering temperature of 1100 °C, while lower sintering temperatures resulted in the formation of secondary phases, which adversely affected the material's properties. As the sintering temperature increased, the grains grew larger, crystallinity improved, and secondary phases were diminished. Magnetic measurements indicated that saturation magnetisation increased with higher sintering temperature, likely due to grain coarsening and reduced surface effects. Unexpectedly, the resistivity showed an unusual increase with rising sintering temperatures, which can be attributed to the presence of secondary phases at lower sintering temperatures and the grain size enlargement in the pure PBMO system at higher sintering temperatures. Higher sintering temperatures may also modify the microstructure, such as by creating oxygen vacancies or porosity, leading to a shift of T_{MI} to lower values. Another notable outcome from this work is that the T_C of PBMO was found to be above room temperature, highlighting the effectiveness of this newly developed thermal treatment method in tuning the physical behaviour of the PBMO samples.

Acknowledgments

This research was fully funded and supported by the Ministry of Higher Education Malaysia (MOHE), under the Fundamental Research Grant Scheme (FRGS/1/2024/STG05/UPM/02/3). The authors are grateful to the support staff who assisted in the characterisation measurements and for the facilities provided by Universiti Putra Malaysia.

Author Contributions

Conceptualization, X.T.H., K.P.L. and L.N.L.; methodology, X.T.H, K.P.L., L.N.L and J.H.; software, X.T.H., K.P.L., L.N.L. and J.H.; validation, X.T.H, K.P.L., L.N.L., J.H., M.M.A.K., S.K.C., M.K.S., N.M.H., N.R., A.H.S., A.D. ; formal analysis, X.T.H., K.P.L and J.H.; investigation, X.T.H, K.P.L., L.N.L., J.H., N.M.H., N.R., A.D. ; resources, K.P.L., M.M.A.K., S.K.C., M.K.S. and A.H.S.; data curation, X.T.H., K.P.L. and J.H.; writing—original draft preparation, X.T.H; writing—review and editing, X.T.H., K.P.L. and L.N.L.; visualization, X.T.H., K.P.L. and L.N.L.; supervision, K.P.L., M.M.A.K, S.K.C., M.K.S. and A.H.S. ; project administration, K.P.L., M.M.A.K., S.K.C., M.K.S. and A.H.S. ; funding acquisition, K.P.L., M.M.A.K., S.K.C., M.K.S., A.H.S. All authors have read and agreed to the published version of the manuscript.

Funding

This research was fully funded and supported by the Ministry of Higher Education Malaysia (MOHE), under the Fundamental Research Grant Scheme (FRGS/1/2024/STG05/UPM/02/3).

Conflicts of Interest

The authors declare no conflict of interest.

References

Aguilar, C., Diosa, J., Mosquera, E., & Rodríguez-Páez, J. (2020). Study of the structural and optical properties of nanoparticles of $Pr_{1-x}Sr_xMnO_3$ (x= 0.1, 0.2, 0.3, 0.4 and 0.5) obtained by a modified polymer complex method. *Materials Science and Engineering: B, 260*, 114617. https://doi.org/10.1016/j.mseb.2020.114617

Bouzayen, A., Elghoul, A., Krichene, A., Boudjada, N. C., & Boujelben, W. (2023). Impact of sintering temperature on the structural, magnetic and magnetocaloric properties in $La_{0.75}Eu_{0.05}Sr_{0.2}MnO_3$ manganite. *Journal of Alloys and Compounds, 952*, 169986. https://doi.org/10.1016/j.jallcom.2023.169986

Christopher, B., Rao, A., Nagaraja, B., Prasad, K. S., Okram, G., Sanjeev, G., Petwal, V. C., Verma, V. P., Dwivedi, J., & Poornesh, P. (2018). Correlation between structural and transport properties of electron beam irradiated $PrMnO_3$ compounds. *Solid State Communications, 270*, 30-37. https://doi.org/10.1016/j.ssc.2017.11.007

Dippong, T., Levei, E. A., Deac, I. G., Petean, I., & Cadar, O. (2022). Dependence of structural, morphological and magnetic properties of manganese ferrite on Ni-Mn substitution. *International Journal of Molecular Sciences, 23*(6), 3097. https://doi.org/10.3390/ijms23063097

dos Santos-Gómez, L., Zamudio-García, J., Caizán-Juanarena, L., Porras-Vázquez, J. M., & Marrero-López, D. (2024). Design and optimization of self-assembled nanocomposite electrodes for SOFCs. *Journal of Power Sources, 613*, 234866. https://doi.org/10.1016/j.jpowsour.2024.234866

Fan, L., Liu, L., Wang, Y., Huo, H., & Xiong, Y. (2014). A novel processing method of $Sr_{0.7}Y_{0.3}CoO_{2.65-\delta}$ cathode for intermediate temperature solid oxide fuel cells. *Ceramics International, 40*(3), 4939-4944. https://doi.org/10.1016/j.ceramint.2013.10.088

Gamzatov, A., Batdalov, A., Abdulkadirova, N., Aliev, A., Khovaylo, V., Thanh, T., Dung, N., & Yu, S.-C. (2023). Giant magnetothermal anomalies and direct measurements of the magnetocaloric effect in $Pr_{0.7}Sr_{0.3-x}Ba_xMnO_3$ manganites. *Journal of Alloys and Compounds, 964*, 171330. https://doi.org/10.1016/j.jallcom.2023.171330

Hanen, R., Mleiki, A., Rahmouni, H., Guermazi, N., Khirouni, K., & Cheikhrouhou, A. (2020). Study of electrical properties of $(Pr/Ca/Pb)MnO_3$ ceramic. *Journal of Materials Science: Materials in Electronics, 31*, 16830-16837. https://doi.org/10.1007/s10854-020-04237-2

Hizi, W., Rahmouni, H., Gorji, N. E., Guesmi, A., Ben Hamadi, N., Khezami, L., Dhahri, E., Khirouni, K., & Gassoumi, M. (2022). Impact of sintering temperature on the electrical properties of $La_{0.9}Sr_{0.1}MnO_3$ manganite. *Catalysts, 12*(3), 340. https://doi.org/10.3390/catal12030340

Hon, X. T., Lau, L. N., Lim, K. P., Kechik, M. M. A., Chen, S. K., Shabdin, M. K., Miryala, M., & Shaari, A. H. (2024). The magnificent manifestation of $Nd_{0.7}Sr_{0.3}MnO_3$ ceramics: A comprehensive exploration of different wet chemical routes via sol-gel and thermal treatment methods. *Journal of Alloys and Compounds, 1004*, 175733. https://doi.org/10.1016/j.jallcom.2024.175733

Hon, X. T., Lau, L. N., Lim, K. P., Wong, Y. J., Ishak, A. N., Kechik, M. M. A., Chen, S. K., Shabdin, M. K., & Shaari, A. H. (2023). Thermal treatment method: A novel approach to prepare $Nd_{0.7}Sr_{0.3}MnO_3$ manganite. *Physica B: Condensed Matter, 650*, 414565. https://doi.org/10.1016/j.physb.2022.414565

Kekade, S. S., Yadav, P., Thombare, B. R., Dusane, P. R., Phase, D., Choudhari, R., & Patil, S. (2019). Effect of sintering temperature on electronic properties of nanocrystalline $La_{0.7}Sr_{0.3}MnO_3$. *Materials Research Express, 6*(9), 096108. https://doi.org/10.1088/2053-1591/ab2f27?urlappend=%3Futm_source%3Dresearchgate.net%26utm_medium%3Darticle

Khelifi, M., M'nassri, R., Selmi, A., Rahmouni, H., Khirouni, K., Boudjada, N. C., & Cheikhrouhou, A. (2017). Investigation of magnetic and transport properties of PrCa(MnCo)O prepared by solid state process. *Journal of Magnetism and Magnetic Materials, 423*, 20-26. https://doi.org/10.1016/j.jmmm.2016.09.069

Lakouader, A., Hadouch, Y., Mezzane, D., Laguta, V., Dolocan, V. O., Novak, N., Hajji, L., Razumnaya, A., Alimoussa, A., & Kutnjak, Z. (2023). Impact of polymeric precursor and auto-combustion on the structural, microstructural, magnetic, and magnetocaloric properties of $La_{0.8}Sr_{0.2}MnO_3$. *Journal of Magnetism and Magnetic Materials, 586*, 171225. https://doi.org/10.1016/j.jmmm.2023.171225

Ling, F., Zhang, H., Li, L., Yu, P., Li, Y., Yang, S., & Chen, Q. (2020). Effect of sintering temperature on structural and electrical transport properties of $La_{0.7}Ca_{0.28}K_{0.02}MnO_3$ ceramics. *Ceramics International, 46*(16), 25949-25955. https://doi.org/10.1016/j.ceramint.2020.07.082

M'nassri, R., Selmi, A., Boudjada, N. C., & Cheikhrouhou, A. (2017). Field dependence of magnetocaloric properties of 20% Cr-doped $Pr_{0.7}Ca_{0.3}MnO_3$ perovskite. *Journal of Thermal Analysis and Calorimetry, 129*, 53-64. https://doi.org/10.1007/s10973-017-6110-1

Malti, A., Kardani, A., & Montazeri, A. (2021). An insight into the temperature-dependent sintering mechanisms of metal nanoparticles through MD-based microstructural analysis. *Powder Technology, 386*, 30-39. https://doi.org/10.1016/j.powtec.2021.03.037

Matheswaran, P., Rajasekhar, M., & Subramania, A. (2017). Assisted combustion synthesis and characterization of $Pr_{0.6}Sr_{0.4}MnO_{3\pm\delta}$ nano crystalline powder as cathode material for IT-SOFC. *Ceramics International, 43*(1), 988-991. https://doi.org/10.1016/j.ceramint.2016.10.030

Mohamed, Z., Shahron, I. S., Ibrahim, N., & Maulud, M. F. (2020). Influence of ruthenium doping on the crystal structure and magnetic properties of $Pr_{0.67}Ba_{0.33}Mn_{1-x}Ru_xO_3$ manganites. *Crystals, 10*(4), 295. https://doi.org/10.3390/cryst10040295

Ngida, R. E., Zawrah, M., Khattab, R., & Heikal, E. (2019). Hydrothermal synthesis, sintering and characterization of nano La-manganite perovskite doped with Ca or Sr. *Ceramics International, 45*(4), 4894-4901. https://doi.org/10.1016/j.ceramint.2018.11.188

Qi, L., Li, Y., Yu, P., Wang, X., Li, Y., Gao, Y., Yang, Y., Wu, D., Zhang, H., & Chen, Q. (2021). Exploring the electrical transport properties of $La_{0.67}Ca_{0.33}MnO_3$ at different sintering temperatures. *Journal of Materials Science: Materials in Electronics, 32*(11), 14164-14173. https://doi.org/10.1007/s10854-021-05943-1

Rosić, M., Kljaljević, L., Jordanov, D., Stoiljković, M., Kusigerski, V., Spasojević, V., & Matović, B. (2015). Effects of sintering on the structural, microstructural and magnetic properties of nanoparticle manganite $Ca_{1-x}Gd_xMnO_3$ (x = 0.05, 0.1, 0.15, 0.2). *Ceramics International, 41*(10), 14964-14972. https://doi.org/10.1016/j.ceramint.2015.08.041

Shogh, S., & Eshraghi, M. (2019). The effect of particle size on the structural, magnetic and electrical properties of $La_{0.9}Ba_{0.1}MnO_3$ manganite samples. *Phase Transitions, 92*(11), 949-959. https://doi.org/10.1080/01411594.2019.1678036

Taboada-Moreno, C., Sánchez-De Jesús, F., Pedro-García, F., Cortés-Escobedo, C., Betancourt-Cantera, J., Ramírez-Cardona, M., & Bolarín-Miró, A. (2020). Large magnetocaloric effect near to room temperature in Sr doped $La_{0.7}Ca_{0.3}MnO_3$. *Journal of Magnetism and Magnetic Materials, 496*, 165887. https://doi.org/10.1016/j.jmmm.2019.165887

Telegin, A., & Sukhorukov, Y. (2022). Magnetic semiconductors as materials for spintronics. *Magnetochemistry, 8*(12), 173. https://doi.org/10.3390/magnetochemistry8120173

Ur Rehman, Z., Anwar, M., & Koo, B. H. (2015). Influence of barium doping on the magnetic and magnetocaloric properties of $Pr_{1-x}Ba_xMnO_3$. *Journal of Superconductivity and Novel Magnetism, 28*, 1629-1634. https://doi.org/10.1007/s10948-014-2933-1

Wang, Z., Jiang, J., Gu, X., Han, J., Liang, X., Wang, Y., Chen, Z., Wang, H., & Liu, X. (2024). Large temperature coefficient of resistivity (TCR) of $La_{0.67}Ca_{0.33}MnO_3$ polycrystalline ceramics improved by optimizing sintering temperatures. *Ceramics International, 50*(7), 10160-10170. https://doi.org/10.1016/j.ceramint.2023.12.326

Wu, D., Zhang, H., Li, L., Qi, L., Gao, Y., Yang, Y., & Chen, Q. (2021). Effect of sintering temperature on structure and electrical transport properties of $La_{0.7}Ca_{0.26}Na_{0.04}MnO_3$ ceramics. *Ceramics International, 47*(9), 12716-12724. https://doi.org/10.1016/j.ceramint.2021.01.131

Xia, W., Pei, Z., Leng, K., & Zhu, X. (2020). Research progress in rare earth-doped perovskite manganite oxide nanostructures. *Nanoscale Research Letters, 15*, 1-55. https://doi.org/10.1186/s11671-019-3243-0

Zhang, J., Chen, X., Zhang, Q., Han, F., Zhang, J., Zhang, H., Zhang, H., Huang, H., Qi, S., & Yan, X. (2018). Magnetic anisotropy controlled by distinct interfacial lattice distortions at the $La_{1-x}Sr_xCoO_3/La_{2/3}Sr_{1/3}MnO_3$ interfaces. *ACS applied materials & interfaces, 10*(47), 40951-40957. https://doi.org/10.1021/acsami.8b14981